



CHORUS

This is the accepted manuscript made available via CHORUS. The article has been published as:

Predicting High Harmonic Ion Cyclotron Heating Efficiency in Tokamak Plasmas

D. L. Green, L. A. Berry, G. Chen, P. M. Ryan, J. M. Canik, and E. F. Jaeger

Phys. Rev. Lett. **107**, 145001 — Published 26 September 2011

DOI: [10.1103/PhysRevLett.107.145001](https://doi.org/10.1103/PhysRevLett.107.145001)

1 **Predicting high harmonic ion cyclotron heating efficiency in**
2 **Tokamak plasmas**

3 D. L. Green,* L. A. Berry, G. Chen, P. M. Ryan, and J. M. Canik

4 *Oak Ridge National Laboratory, P.O. Box 2008,*

5 *Oak Ridge, Tennessee 37831-6169, USA*

6 E. F. Jaeger

7 *XCEL Engineering Inc., 1066 Commerce Park Dr., Oak Ridge, TN 37830, USA*

8 (Center for Simulation of Wave-Plasma Interactions SciDAC)

Abstract

Observations of improved radio frequency (RF) heating efficiency in ITER relevant high-confinement (H-) mode plasmas on the National Spherical Tokamak Experiment (NSTX) are investigated by whole-device linear simulation. The steady-state RF electric field is calculated for various antenna spectra and the results examined for characteristics that correlate with observations of improved or reduced RF heating efficiency. We find that launching toroidal wave-numbers that give fast-wave propagation in the scrape-off plasma excites large amplitude ($\sim\text{kVm}^{-1}$) coaxial standing modes between the confined plasma density pedestal and conducting vessel wall. Qualitative comparison with measurements of the stored plasma energy suggests that these modes are a probable cause of degraded heating efficiency.

9 PACS numbers: 52.35.-g,52.50.Qt,52.55.Fa,52.65.-y

10 INTRODUCTION

11 Our understanding of magnetically confined nuclear fusion has progressed to a state
12 where net energy production is within reach. The next step towards achieving this goal is
13 ITER[1], a reactor scale Tokamak currently under construction in Cadarache, France. To
14 achieve fusion, ITER's plasma will be heated to ~ 20 keV using 50 MW of external heating
15 power from combined neutral beam injection (NBI) and both electron- and ion-cyclotron
16 (IC) frequency RF waves. The RF waves are also used to drive current in order to control the
17 background magnetic field and non-inductively sustain the plasma. In this paper we show
18 that RF power in the IC frequency regime can excite normal modes of the plasma edge,
19 whose presence correlates with decreased heating efficiency. This investigation is enabled by
20 advances to the state-of-the-art in predictive computer simulation of IC heating and current
21 drive (CD) for Tokamak plasmas relevant to ITER. Specifically, we use the first simulation to
22 solve for the linear RF wave fields in a realistic whole-device configuration while maintaining
23 all required kinetic physics for ITER relevant heating scenarios. We solve self consistently
24 for wave fields in both the well-confined core plasma and poorly confined scrape-off plasma
25 (see Fig. 2). An ability to predict efficiency and performance of IC heating on ITER, and
26 thus optimize heating scenarios, will be essential to the development of an economically
27 viable magnetic confinement fusion power source. Such an ability will require high fidelity
28 whole-device simulation with the work presented here being a step toward that goal. In
29 addition, this work is relevant to general plasma wave propagation regimes where kinetic
30 effects and strong density gradients across a boundary of open and closed magnetic field
31 lines are important, e.g., kinetic Alfvén waves at the Earth's magnetopause[2]. Significant
32 progress in predicting the plasma response to ICRF waves in Tokamak plasmas has been
33 achieved[3–5], largely coupled to the availability of leadership class computing facilities such
34 as the Jaguar machine at the National Center for Computational Sciences. ITER D-T
35 scenarios will be fast-wave heated at the first harmonic of deuterium and second of tritium.
36 While high-harmonic fast-wave (HHFW) heating is used on the National Spherical Tokamak
37 Experiment (NSTX)[6], for the present investigation of coupling fast-wave power from the
38 antenna to the core plasma, NSTX provides a suitable testbed. Here we compare results
39 from the whole-device (2- and 3-D, antenna-to-core) simulation with recent experimental
40 observations of improved IC heating efficiency on NSTX for a NBI H-mode scenario.

41 The NSTX IC antenna consists of a 12 strap phased array which toroidally spans $\sim 90^\circ$
 42 (see Fig. 3) and is capable of launching 6 MW of electromagnetic fast-wave power at 30 MHz.
 43 The fast-wave is typically strongly damped on electrons in a single pass through the core
 44 plasma via transit time magnetic pumping and electron Landau damping[7]. Using six de-
 45 coupled power sources gives good control over the toroidal wave-number (k_ϕ) of the launched
 46 wave. Experimental observations on NSTX show poor heating efficiency for small k_ϕ in both
 47 L-[8] and H-mode[9] scenarios. Heating efficiency was determined in these experiments by
 48 the correlation between launched RF power and measured increase in plasma stored en-
 49 ergy for electrons (W_e) using a Thomson scattering diagnostic for kinetic electron pressure
 50 (c.f. Fig. 2 of Ref. [8]). Since small k_ϕ waves are desired for their current drive efficiency
 51 characteristics[10], understanding why RF heating efficiency is poor for small k_ϕ is of im-
 52 portance. The dependence of heating efficiency on the launched k_ϕ has been interpreted
 53 by Refs. [8, 11] in terms of the location where the fast-wave transitions from evanescent in
 54 the antenna near-field to a propagating wave, i.e., the cutoff/onset location for fast-wave
 55 propagation. For scenarios with improved heating efficiency, the hypothesis is that this
 56 location is inside the core plasma (high temperature and pressure) defined by closed mag-
 57 netic flux surfaces (c.f., Fig. 2). Poor efficiency heating scenarios are expected to have the
 58 onset location in the scrape-off plasma (low temperature and pressure) that exists on open
 59 magnetic field lines near the wall and encompasses the antenna. This is explained using a
 60 0-D dispersion relation analysis where, given the confining magnetic field strength (B) and
 61 launched toroidal wave-number, the onset density for fast-wave propagation is shown to be
 62 approximately proportional to Bk_ϕ^2/ω where ω is the angular RF frequency. Due to the $\frac{1}{R}$
 63 fall off in toroidal magnetic field strength with radius (R) from the device center stack (c.f.,
 64 Fig. 3), launching a larger k_ϕ or increasing B effectively pushes the onset location away from
 65 the antenna and further into the plasma. It is suggested by Refs. [8, 11] that fast-wave prop-
 66 agation in the scrape-off plasma can cause decreased RF heating efficiency due to possible
 67 formation of coaxial modes and damping of these edge waves via sheath effects or collisions
 68 in the low temperature plasma.

69 By retaining all relevant kinetic effects for the hot core plasma, including realistic density
 70 and temperature gradients between the core and scrape-off plasmas, and solving for the
 71 wave field out to the limiting vacuum vessel structures, we show that fast-wave propagation
 72 in the edge plasma is a plausible explanation for the observed degradation in RF heating

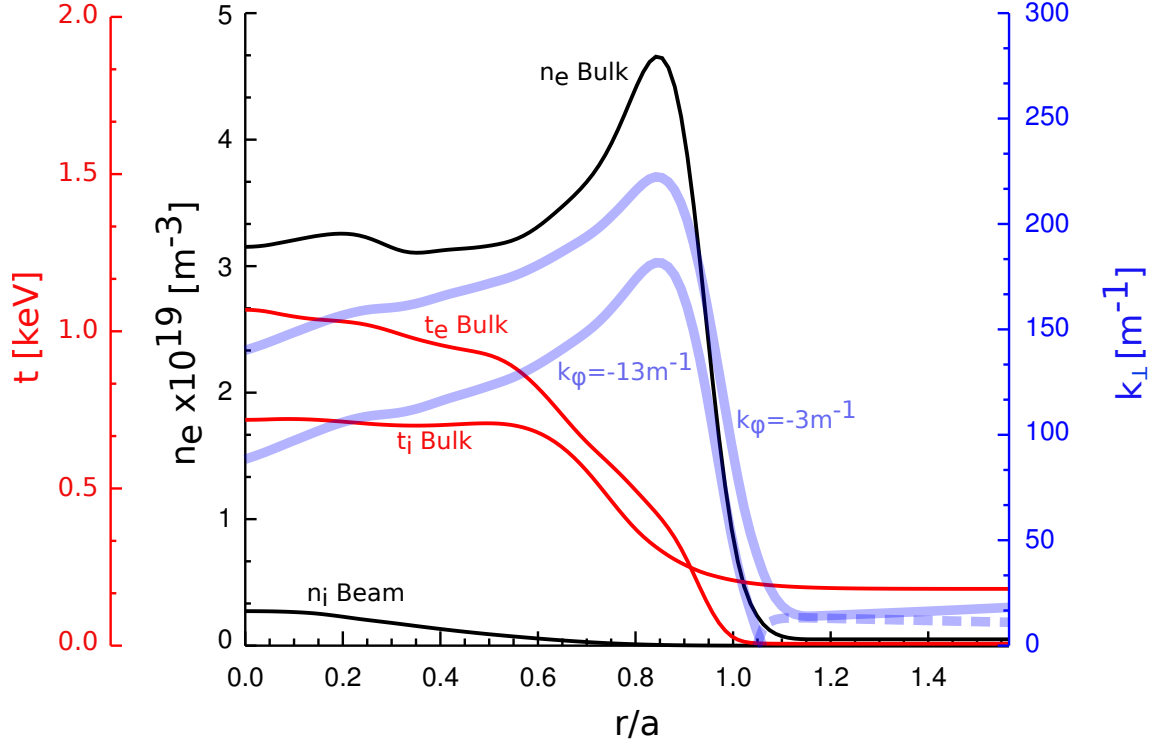


FIG. 1. Midplane profiles for NSTX shot 130608 as used in the simulations presented here. Electron density (n_e) and temperature (T_e) are from multi-point Thomson scattering (MPTS) data, ion temperature (T_i) is from charge exchange recombination spectroscopy (CHERS) data and the NBI fast-ion density (n_i) is from TRANSP[12] simulation. $a = 1.52$ m is the minor radius.

73 efficiency. The following full-wave analysis reveals RF excited normal modes. These modes
 74 are not seen in linear plasma wave dispersion relation or ray tracing approaches.

75 SIMULATION DETAILS

76 The simulation of RF wave propagation in hot plasmas is complicated by a non-local
 77 plasma response. Assuming a linear medium where the wave energy is much less than the
 78 plasma stored energy, the problem is typically Fourier transformed in space and time to
 79 a frequency domain Helmholtz wave equation containing a hot plasma dielectric tensor[13]
 80 that, due to the spatial non-locality, has a dependence on wave-number. Furthermore, in
 81 the magnetised plasmas considered here, the medium is highly anisotropic. As such, the
 82 dielectric is separated into directions parallel (\parallel) and perpendicular (\perp) to the confining
 83 magnetic field. However, the inclusion of a scrape-off plasma requires solving the Helmholtz

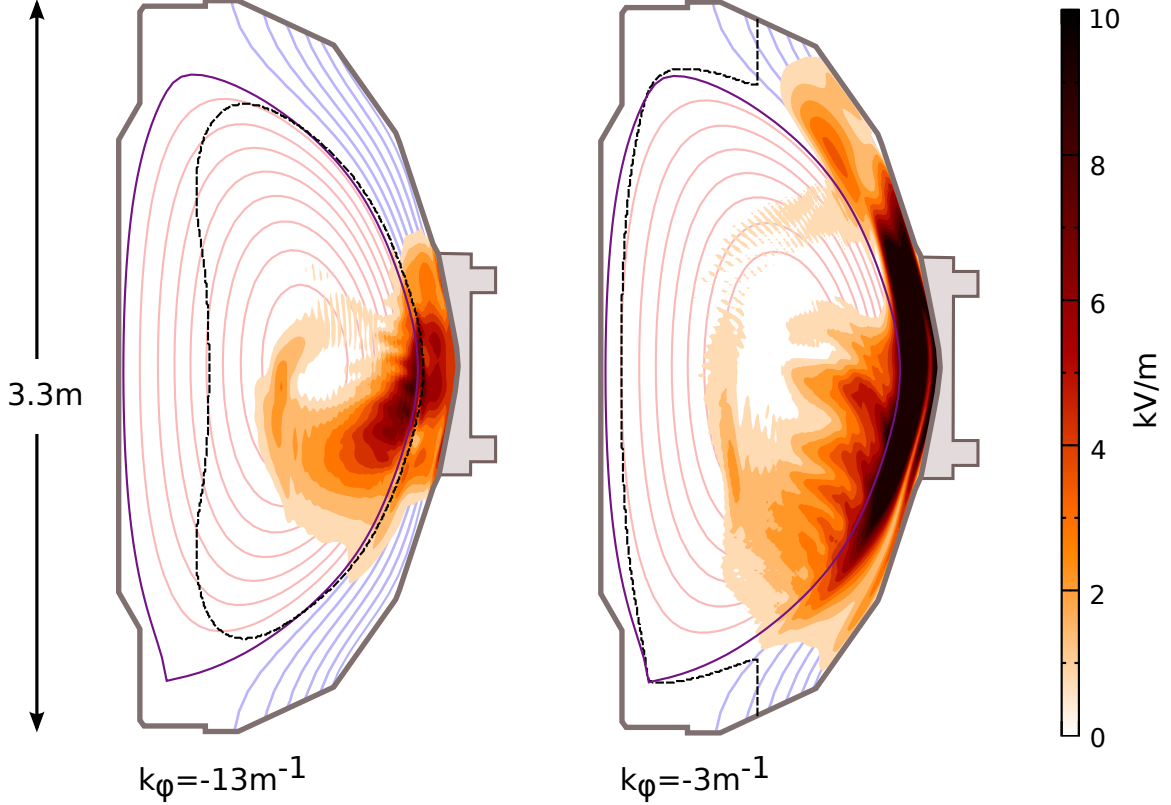
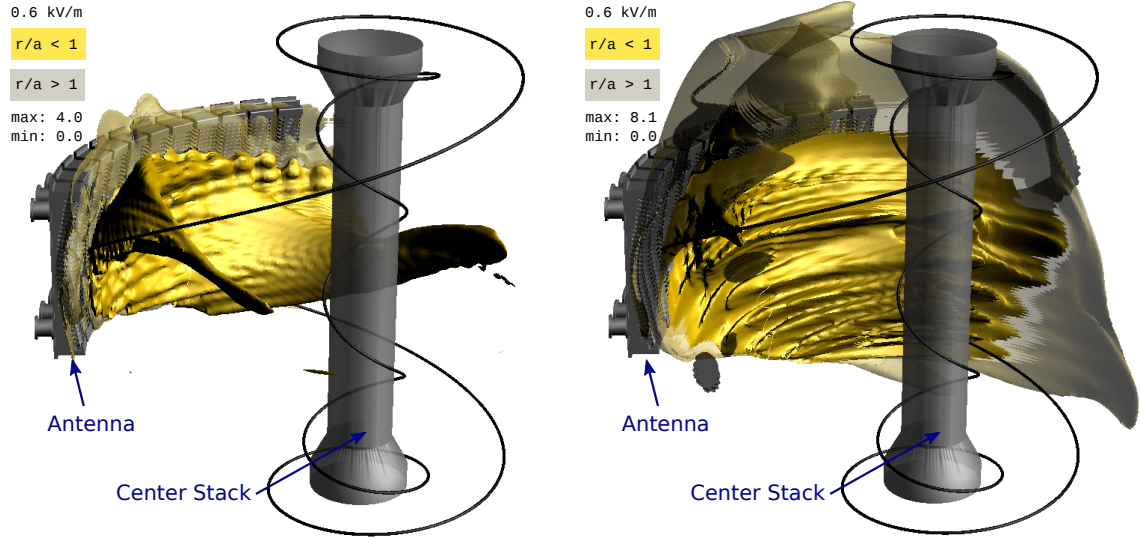


FIG. 2. 2-D AORSA simulation results of the steady-state wave electric field amplitude for HHFW on NSTX. The dashed line shows an approximate fast-wave cutoff based on a 0-D dispersion calculation using $k_{\parallel} \approx k_{\phi} = n_{\phi}/R$. The separatrix is shown in purple, closed magnetic flux surfaces of the core plasma are in red and open flux surfaces of the scrape-off plasma are in blue.

84 system across the boundary between closed and open magnetic field lines (separatrix, c.f.,
 85 Fig. 2). Most hot plasma simulations use magnetic flux surface coordinates which break
 86 down at the separatrix. For this reason we utilize a spectral representation in all spatial
 87 directions via the All ORders Spectral Algorithm (AORSA)[3]. AORSA uses Cartesian coor-
 88 dinates such that the directions for the spectral decomposition of the $\vec{\nabla} \times \vec{\nabla} \times$ piece of the
 89 Helmholtz equation are chosen independently of the background magnetic field. Therefore,
 90 the boundary between open and closed magnetic field lines is not significant in AORSA and
 91 the addition of a scrape-off plasma is straight forward, although limited as will be discussed.
 92 Also, for the NSTX HHFW heating scenarios considered in this paper, the ion Larmor radius
 93 (ρ_i) can exceed the perpendicular wavelength ($k_{\perp}\rho_i \geq 1$) and the ion cyclotron harmonic
 94 number (l) can be as high as 18. Being spectral (non-local) in all directions, AORSA ensures
 95 these physics are included. Such an approach produces a large dense matrix that require



(a) $\pm 180^\circ$ antenna phasing, dominant mode

$$k_\phi = \pm 13 \text{ m}^{-1}.$$

(b) -30° antenna phasing, dominant mode

$$k_\phi = -3 \text{ m}^{-1}.$$

FIG. 3. 3-D AORSA results for the steady-state wave electric field amplitude. The gold (solid) and gray (transparent) contours are 0.6 kV m^{-1} and are inside and outside the LCFS respectively. The antenna, center stack and sample magnetic field line trajectory are shown. Figures were created using VisIt (<http://visit.llnl.gov/>).

96 leadership class computing facilities to factor and invert. The 3-D simulation presented here
 97 required ~ 20 k processor hours with each 2-D mode producing a matrix of ~ 1 TB.

98 While extending AORSA to include a scrape-off plasma avoids boundary condition match-
 99 ing problems associated with coupling a dedicated scrape-off plasma code to a core plasma
 100 code, it does come at a high computational cost that limits the scrape-off plasma resolution.
 101 This restricts us to qualitative comparison with experiment. The low resolution limitation
 102 is primarily due to the uniform spatial grid used by AORSA. At present there is no variable
 103 grid formulation of the Fourier spectral method compatible with the hot plasma dielectric
 104 tensor, and as such we cannot yet resolve the fine scale (mm) features of the antenna and
 105 Faraday shield.

106 Figure 1 shows the background density and temperature profiles used for the simulation.
 107 These were constructed to best match available experimental data from NSTX shot 130608
 108 presented in Ref. [9]. This shot heats a NBI deuterium plasma with 1.8 MW of ICRF power.
 109 The equilibrium magnetic field is from an EFIT[14] reconstruction with a plasma current

110 of 0.99 MA (0.54 T on axis toroidal magnetic field strength). This is a H-mode shot where
 111 the density and temperature profiles exhibit a steep density gradient near the last closed
 112 magnetic flux surface (LCFS). 1-D midplane electron density (n_e) profiles are measured
 113 with Thompson scattering in the core and with microwave reflectometry in the scrape-off
 114 plasma. These data are mapped along closed flux surfaces to give 2-D profiles for the core
 115 plasma. For estimating the 2-D scrape-off n_e profile experimental midplane data near the
 116 LCFS are fit giving a decay of the form $n_e(\delta r) = 0.039 + 3.6 \exp(-147.0\delta r^{1.4}) \times 10^{19} \text{ m}^{-3}$
 117 where δr is distance from the LCFS. This approach gives profiles that decay to a constant
 118 $n_e = 3.9 \times 10^{17} \text{ m}^{-3}$ within a few cm of the LCFS. In addition, this minimum value of
 119 n_e in the scrape-off plasma is above that required for propagation of the short wavelength
 120 slow-wave mode[13]. As stated above, resolving such short wavelength modes will require
 121 improvements to AORSA. A similar procedure is followed for the bulk temperatures and NBI
 122 fast-ion density with the profiles shown in Fig. 1. The NBI fast-ion temperature profile is
 123 set to a flat 20 keV.

124 SIMULATION RESULTS

125 Figure 2 shows 2-D AORSA results for single toroidal modes $n_\phi = -22$, and -5 ($k_\phi =$
 126 -13 m^{-1} , -3 m^{-1}) corresponding to the dominant mode of the antenna spectrum for $\pm 180^\circ$
 127 and -30° phasing respectively. A clear dependence on the launched toroidal wave-number
 128 can be seen. For large k_ϕ (-13 m^{-1}) the fast-wave is seen to be evanescent in the scrape-off
 129 plasma and begins to propagate at the core plasma where the density reaches the onset
 130 value (dashed line in Fig. 2). The wave is seen to penetrate the core plasma and is refracted
 131 back towards the low-field side before being absorbed primarily on electrons (56.5%) and
 132 NBI fast-ions (36.1%). For small k_ϕ (-3 m^{-1}), there are large amplitude electric wave fields
 133 between the core plasma density gradient near the last closed magnetic flux surface and the
 134 antenna/vessel wall. The field magnitude plot shows a null indicating a standing coaxial
 135 mode as predicted by Ref. [8].

136 Figure 3 shows the 0.6 kV m^{-1} contour of the 3-D electric wave field magnitude as calcu-
 137 lated from the sum over $-50 \leq n_\phi \leq 50$ with toroidal mode spectral weightings calculated
 138 for antenna phasings of $\pm 180^\circ$ and -30° . Fig. 3a shows little fast-wave presence in the
 139 scrape-off plasma, and significant penetration of the core plasma. Fig. 3b shows consider-

140 able fast-wave in the scrape-off plasma and poor core penetration.

141 SUMMARY AND CONCLUSIONS

142 The first whole-device 3-D HHFW simulation to include realistic edge density profiles for
143 a H-mode plasma, while retaining all-orders in $k_{\perp}\rho_i$ and harmonic number are presented.
144 In addition to the typical fast-wave damping on electrons and NBI fast-ions in the core
145 plasma is a standing coaxial mode in the scrape-off plasma seen to be excited to large
146 amplitude. Assuming the large amplitude coaxial mode is damped on collisions or non-linear
147 phenomena[15] (parasitic loss of power that would otherwise end up in the core plasma), we
148 see qualitative agreement between simulation and experiment that supports the hypothesis
149 that excitation of coaxial edge modes reduce ICRF heating efficiency.

150 The conclusions of this work have implications for ITER, where the separatrix-wall dis-
151 tance is large (10 to 20 cm). It may prove difficult to control the edge density in such a
152 large region to below that for fast-wave propagation. Assuming an electron density at the
153 separatrix in ITER of $n_0 = 1 \times 10^{19} \text{ m}^{-3}$, with a decay in the scrape-off plasma of the
154 form $n(\delta r) = n_0 \exp(-\delta r/l_{SOL})$ where δr is the distance from the LCFS and $l_{SOL} = 4 \text{ cm}$
155 is the scrape-off plasma decay length, the onset location for fast-wave propagation for the
156 dominant mode for -90° antenna phasing ($n_\phi = -32$, $k_\phi = -3.84 \text{ m}^{-1}$) is 11 cm from the
157 wall, well within the scrape-off plasma. Therefore, optimizing the scrape-off plasma density
158 profile will be important for ICRF heating efficiency on ITER.

159 Future work will focus on quantitative comparison of the scrape-off plasma electric field
160 magnitudes with direct experimental observation and further improving predictive capability
161 for ITER. This will require improving the resolution in the scrape-off plasma to resolve the
162 antenna and Faraday shield. Also, the linear wave amplitude in the scrape-off plasma will
163 be provided as invaluable input data to non-linear simulations.

164 The authors wish to thank Benoit P. LeBlanc for providing TRANSP NBI profile data.
165 This research used resources of the Oak Ridge Leadership Computing Facility, located in
166 the National Center for Computational Sciences at Oak Ridge National Laboratory, and the
167 National Energy Research Scientific Computing Center supported by the Office of Science of
168 the Department of Energy under Contracts DE-AC05-00OR22725 and DE-AC02-05CH11231
169 respectively.

-
- 170 * greendl1@ornl.gov
- 171 [1] N. Holtkamp, Fusion Engineering and Design **82**, 427 (2007), proceedings of the 24th Sym-
172 posium on Fusion Technology - SOFT-24.
- 173 [2] J. R. Johnson and C. Z. Cheng, Geophys. Res. Lett. **24**, 1423 (1997).
- 174 [3] E. F. Jaeger, L. A. Berry, J. R. Myra, D. B. Batchelor, E. D’Azevedo, P. T. Bonoli, C. K.
175 Phillips, D. N. Smithe, D. A. D’Ippolito, *et al.*, Phys. Rev. Lett. **90**, 195001 (2003).
- 176 [4] E. Jaeger, R. Harvey, L. Berry, J. Myra, R. Dumont, C. Phillips, D. Smithe, R. Barrett,
177 D. Batchelor, P. Bonoli, M. Carter, E. D’azevedo, D. D’ippolito, R. Moore, and J. Wright,
178 Nuclear Fusion **46**, S397 (2006).
- 179 [5] D. L. Green, E. F. Jaeger, and L. A. Berry (RF-SciDAC Team), Journal of Physics: Confer-
180 ence Series **180**, 012058 (2009).
- 181 [6] M. Ono, S. Kaye, Y.-K. Peng, G. Barnes, W. Blanchard, M. Carter, J. Chrzanowski, L. Dudek,
182 R. Ewig, D. Gates, R. Hatcher, T. Jarboe, S. Jardin, D. Johnson, R. Kaita, M. Kalish, *et al.*
183 (NSTX Team), Nuclear Fusion **40**, 557 (2000).
- 184 [7] M. Ono, Physics of Plasmas **2**, 4075 (1995).
- 185 [8] J. Hosea, R. E. Bell, B. P. LeBlanc, C. K. Phillips, G. Taylor, E. Valeo, J. R. Wilson, E. F.
186 Jaeger, P. M. Ryan, J. Wilgen, *et al.* (NSTX Team), Physics of Plasmas **15**, 056104 (2008).
- 187 [9] G. Taylor, R. E. Bell, J. C. Hosea, B. P. LeBlanc, C. K. Phillips, M. Podesta, E. J. Valeo,
188 J. R. Wilson, J.-W. Ahn, G. Chen, D. L. Green, E. F. Jaeger, *et al.* (NSTX Team), Physics
189 of Plasmas **17**, 056114 (2010).
- 190 [10] M. Brambilla, *Kinetic Theory of Plasma Waves* (Oxford University Press Inc., New York,
191 1998).
- 192 [11] C. Phillips, R. Bell, L. Berry, P. Bonoli, R. Harvey, J. Hosea, E. Jaeger, B. LeBlanc, P. Ryan,
193 G. Taylor, *et al.* (NSTX Team), Nuclear Fusion **49**, 075015 (2009).
- 194 [12] R. Budny, M. Bell, A. Janos, D. Jassby, L. Johnson, D. Mansfield, D. McCune, M. Redi,
195 J. Schivell, G. Taylor, T. Terpstra, M. Zarnstorff, and S. Zweben, Nuclear Fusion **35**, 1497
196 (1995).
- 197 [13] T. H. Stix, *Waves in plasmas* (Springer-Verlag New York, Inc., 1992).
- 198 [14] S. Sabbagh, S. Kaye, J. Menard, F. Paoletti, M. Bell, R. Bell, J. Bialek, M. Bitter, E. Fredrick-

199 son, D. Gates, A. Glasser, H. Kugel, L. Lao, B. LeBlanc, R. Maingi, *et al.* (NSTX Team),
200 Nuclear Fusion **41**, 1601 (2001).
201 [15] D. A. D'Ippolito and J. R. Myra, Physics of Plasmas **13**, 102508 (2006).